

Metallic Monopole Parasitic Antenna With Circularly Polarized Conical Patterns

Sumit Karki¹, Marco Sabbadini, Khaldoun Alkhalifeh², *Member, IEEE*,
and Christophe Craeye³, *Senior Member, IEEE*

Abstract—In this paper, a new geometry for antenna producing conical patterns with circular polarization is proposed. The symmetrically placed parasitic posts, with different horizontal and vertical segments, around the centrally fed monopole control the circular polarization purity and the angle of maximum gain. The 3-D geometry favors high gain at low elevation angles. A circular ground plane atop a choke ring facilitates easy mounting of a radome and improves gain at lower elevation due to lower backlobe. The all-metal radiator has good mechanical stability and remains impervious to large temperature variations, which is ideal for use in space applications. An application to a Martian transponder at the X-band is also discussed. The measured results of the manufactured antennas show a good agreement with those of the simulated one. Furthermore, the optimization of the antenna design parameters allows the antenna to have high gain and low axial ratio (AR), from high elevation ($\theta_{max} = 35^\circ$) to low elevation ($\theta_{max} = 70^\circ$) angles.

Index Terms—Circular polarization, conical beam, monopole antenna, mutual coupling, parasitic array.

I. INTRODUCTION

CIRCULARLY polarized (CP) conical-beam antennas have been extensively studied in the literature. Such antennas find wide applications in communications between mobile devices and satellites with their uniform elevation patterns over the azimuth plane. This avoids an expensive and mechanically complex system to track the objects in the sky (rendering the tracking system redundant). The azimuthal symmetry allows a wider coverage for the mobile devices. The CP antennas also help to mitigate interference from multipath propagation [1], [2] and reduce the effect of change in polarization due to the Faraday rotation in the ionosphere, especially for frequencies at and below the X-band [3].

Huang [4] proposed the use of a circular patch fed with two or four probes to excite the higher order modes of the circular waveguide. The work provides a useful guide to generate CP conical-beam patterns for different peak directivities using

different substrates and resonant modes. The use of the four probes, however, requires a feeding network adding losses, increasing the overall size, and possibly requiring multiple layers of dielectric substrates. Kawakami *et al.* [5] proposed another CP conical-beam antenna relying on the introduction of four inclined monopole elements placed in a circular array. The inclination angle and the separation between the elements would help generate CP in the desired direction. Even though no phase shifters were required, the antenna still needed a feed network. Lau and Luk [2] presented a wideband CP conical-beam patch antenna using L-probes and apertures connected through a hybrid feed network. However, the antenna has a complex microstrip feeding network [6], which is prone to back radiation.

Recent works show a trend toward simplifying the feed network with a central pin exciting the antenna system. Nakano *et al.* [7] proposed a wideband (3.3–9.6 GHz) CP conical-beam low-profile two-arm spiral antenna. However, it has more than 5 dB azimuth gain variation over the entire bandwidth. Pan and Leung [8] investigated a centrally fed wideband antenna surrounded by eight inclined parasitic dielectric parallelepipeds. The structure is complex [9] and not very robust, making the integration of the dielectric material tedious. In addition, the axial ratio (AR) bandwidth is easily influenced by the size of the ground plane [10]. Qi *et al.* [6] proposed a single-feed circular aperture CP antenna by simultaneously exciting the TM_{01} and TE_{01} orthogonal modes in a circular waveguide to produce CP.

Lin and Wong [9], Yu *et al.* [10], and Xu *et al.* [11] showed similar designs for a centrally fed printed patch, contributing primarily to the horizontal polarization, with loop stubs [9], modified elliptical-ring slots [10], or annular ring slots [11], contributing mainly to the vertical polarization. They employ different resonant modes (mainly TM_{01} and TM_{02} of the patch) to improve the bandwidth of the antennas. The AR of the loop stubs antenna is easily affected by the size of the ground plane, which is not the case for the slot array designs. All of these designs [9]–[11], however, produce high-elevation patterns (θ between 28° and 35°). Reducing the number of loop stubs or elliptical-ring slots effectively lowers the elevation angle but the gain and AR are then sharply degraded [9]. Kumar and Harish [12] proposed a torus knot radiator fed with a central monopole, but the torus knot is complicated to manufacture although it might be easier with additive manufacturing. Also, the gain value is below 3 dB

Manuscript received September 30, 2018; revised April 13, 2019; accepted April 22, 2019. Date of publication May 20, 2019; date of current version August 12, 2019. This work was supported by the Belgian Fund for Scientific Research (FNRS). (*Corresponding author: Sumit Karki.*)

S. Karki, K. Alkhalifeh, and C. Craeye are with the ICTEAM Institute, Université catholique de Louvain, 1348 Louvain-la-Neuve, Belgium (e-mail: sumit.karki@uclouvain.be; khaldoun.alkhalifeh@uclouvain.be; christophe.craeye@uclouvain.be).

M. Sabbadini is with ESA-ESTEC, 2201 Noordwijk, The Netherlands (e-mail: marco.sabbadini@esa.int).

Color versions of one or more of the figures in this paper are available online at <http://ieeexplore.ieee.org>.

Digital Object Identifier 10.1109/TAP.2019.2916737

at the observation angle of $\theta = 30^\circ$. Ohmine *et al.* [13], [14] reported annular-ring microstrip antennas for mobile satellite communication with a high gain at lower elevation angles (gain of at least 3 dB for $30^\circ \leq \theta \leq 60^\circ$). However, it is still difficult to achieve a value of gain higher than 3 dB for $\theta < 60^\circ$.

It is apparent from the literature review that a true CP conical-beam antenna with high gain and low AR for low elevation application is lacking, which is difficult to achieve with planar structures. Chenhu *et al.* [15] proposed a slot array on a truncated cone to generate CP conical beams, whose angle of maximum gain would depend on the tilt angle of the cone. While this design can be adapted to any beam-pointing angle and that the overall gain can reach 5.8 dB, it still needs dielectric support, which needs to conform to the conical structure.

This paper presents a novel and robust antenna design based on parasitic elements placed around the centrally fed monopole, capable of generating excellent CP conical-beam patterns at low elevation. Given the degree of freedom in choosing the height of the parasitic element that aids in sideways radiation, the proposed antenna performs very well at low elevation. Nevertheless, the gain tends to drop at low elevation compared to that at high elevation. This is simply because the solid angle covered by the symmetrical beam over azimuth at low elevation is much larger than that at high elevation for the same elevation beamwidth. Made entirely of metal, the antenna can also be used in harsh climatic conditions, such as for planetary observation.

The use of parasitic elements around a central radiator is also found in electronically steerable parasitic array radiator (ESPAR) antennas [16], [17]. Schlub *et al.* [16] showed how loaded parasitic elements around a centrally excited monopole radiator can be used for beamsteering, but the antenna in [16] was not designed as a conical-beam radiator. Liu *et al.* [17] reported antennas with folded parasitic monopole elements, which are varactor loaded, facing toward the center. The folding of the elements helps to provide a larger capacitive loading, reducing the size of the antenna. However, this antenna is also used for beamscanning over the entire azimuth and is specific to linear polarization. This paper will focus on the generation of smooth conical patterns with circular polarization, with particular attention given to radiation at low elevation.

The remainder of this paper is organized as follows. Section II gives a detailed description of the antenna, its working principle, and the design methodology. Section III provides a parametric study, whereas Section IV discusses the antenna gain optimization. Section V provides a comparison with the measured results of the 3-D printed prototype. Finally, Section VI discusses an application to a Martian transponder, including a square coaxial feed, and also shows the measured results.

II. ANTENNA DESCRIPTION

The newly proposed antenna corresponds to a monopole above a ground plane surrounded by N parasitic posts (see Fig. 1, where $N = 8$). The latter are symmetrically arranged

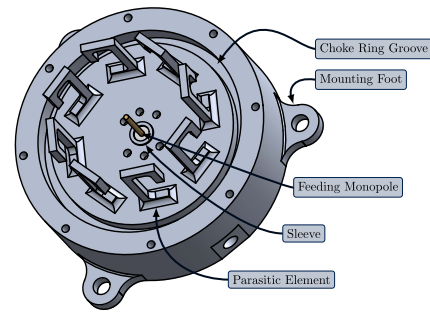


Fig. 1. Perspective view of the monopole parasitic antenna.

around the monopole (rotation by $2\pi/N$) and are protruding from the ground plane. They have a curled (or gamma) shape in order to exhibit horizontal parts that generate horizontally polarized fields and create, together with the radiation from the vertical monopole, conical patterns with circular polarization. The radiating elements are supported by a ground plane, which, in turn, is itself supported by a cylindrical aluminum housing, in which one or several grooves are made. Those grooves can act as choke rings, which tend to stop the current and hence limit backradiation [18], [19]. In practice, multiple choke rings are used [19]. In this paper, only one ring is considered to limit the antenna size. Assuming that sufficient volume is available, a further improvement of backlobes can certainly be achieved using multiple rings, but that optimization is outside the scope of this paper. Finally, a tube surrounding the monopole, called the monopole sleeve, provides a degree of freedom to tune the antenna impedance [20]. The sleeve creates an additional capacitance in parallel with the antenna impedance and allows matching over a wider bandwidth.

A. Working Principle of the Monopole Parasitic Antenna

When only the monopole is present, given the symmetry of the structure, only vertical polarization is obtained. However, a relatively broad conical pattern is expected since monopoles with axial symmetry cannot radiate along their axis in the far field. As is well known, to obtain a good circular polarization, horizontal or skewed components need to be added to the structure. This could be done here using parasitic elements, which: 1) would form an angle with the ground and 2) would be purely horizontal. In the case of the structure considered here, to produce mechanically self-standing elements, it is necessary to connect the parasitics to the ground, preferably using the same (metallic) material. Regarding the use of horizontal parasitics [option 2) above], it is possible to prove, based on symmetry, that practically no current would flow on purely horizontal parasitics. Indeed, a perfect magnetic conductor (PMC) symmetry plane can cross the structure through the pin and the middle of the horizontal parasitics showing that the current at the middle of the parasitics must be zero. Given the rotational symmetry, the horizontal parts must radiate a null at the broadside. The vertical parts radiate like monopoles and hence also produce patterns with zero fields at the broadside. Thus, the antenna naturally radiates a conical pattern.

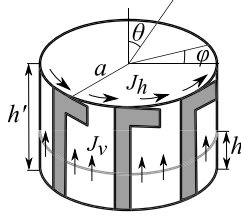


Fig. 2. Current distribution on the cylindrical model of the monopole parasitic antenna.

Let us now consider the connection of the horizontal parasitics, through a vertical metallic post, to the ground. This new configuration helps: (1) to break the symmetry referred to above and (2) to “pump” current from the ground plane to the horizontal part of the parasitics. Based on time-domain simulations, we could observe that, roughly speaking, there is a progressive wave moving upward in the vertical part of the parasitic element, while there is a standing wave on the folded section (see Fig. 4). Moreover, to allow substantial current on the horizontal part, a vertical post at the end of the horizontal structure is added, avoiding sharp ending of current at the end of the horizontal parasitics.

This new geometry, however, raises the issue of potentially strong fields radiated by the vertical parts of the parasitics. In the following, we prove that, if the radius a of the antenna (distance between parasitics and feed) is well chosen, those extra fields can be kept very small, while the fields from the horizontal parts are maximum. This is explained assuming the limit of a large number of parasitics around the monopole (in the examples considered further in this paper, we have 8–14 parasitics). Under that approximation, the currents along the vertical parts of the parasitics are replaced by a cylindrical current sheet J_v , flowing parallel to the axis of the cylinder (see Fig. 2).

Let us now calculate the radiation integral regarding the contribution of J_v on a circular cut of the cylinder at height h , with ϕ being the azimuthal coordinate along the circle (see Fig. 2). For radiation in a direction θ from broadside while omitting multiplicative constants, the radiation integral reads

$$I_v = \int_0^{2\pi} J_v e^{jk(a \cos \phi \sin \theta + h \cos \theta)} \sin \theta d\phi \quad (1)$$

$$= 2\pi e^{jk h \cos \theta} J_v J_0(ka \sin \theta) \sin \theta \quad (2)$$

$$= 2\pi e^{jk h \cos \theta} J_v I_v^\circ \sin \theta \quad (3)$$

where k is the wavenumber, and J_0 is the Bessel function of the first kind and order 0.

The currents on the horizontal parts of the parasitics are approximated as flowing along a circle at height h' (see Fig. 2). The radiation integral reads

$$I_h = \int_0^{2\pi} J_h \cos \phi e^{jk(a \cos \phi \sin \theta + h' \cos \theta)} d\phi \quad (4)$$

$$= 2\pi e^{jk h' \cos \theta} J_h J_1(ka \sin \theta) \quad (5)$$

$$= 2\pi e^{jk h' \cos \theta} J_h I_h^\circ \quad (6)$$

where J_h is the azimuthal current, and J_1 is the Bessel function of the first kind and order 1. I_v° and I_h° in (3) and (6),

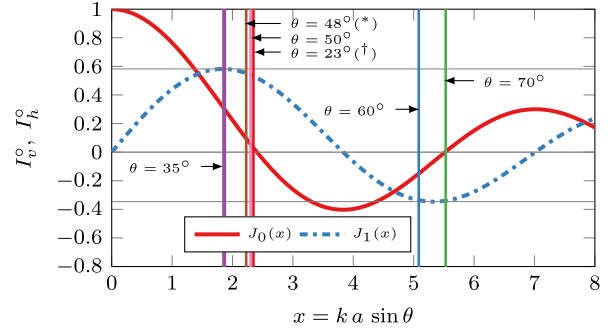


Fig. 3. Normalized radiation integrals for horizontal and vertical polarizations versus antenna radius and direction of the maximum beam. Vertical lines stand for values of $ka \sin \theta$ described in Table III, (*) stands for the values given in Table I, and (†) refers to the secondary maximum for the beam pointed at $\theta = 70^\circ$ in Table III.

respectively, are the normalized radiation integrals, limited to the only factor depending on radius a .

Hence, for a given desired direction of radiation θ , we want the magnitude of I_v to be as small as possible and that of I_h to be as large as possible, so as to maximize the radiation from the horizontal parts of the parasitics and to minimize the radiation from the vertical parts. Based on (2) and (5), this translates into radius a satisfying the following conditions: $x = ka \sin \theta$ needs to be close to a zero of $J_0(x)$ and close to a maximum of $|J_1(x)|$. The vertical lines in Fig. 3 correspond to abscissas x obtained for different designs provided in Section IV, which satisfy well the above-mentioned conditions to allow a good polarization balance. For $\theta = 35^\circ$ and $\theta = 60^\circ$, a significant deviation is observed with respect to the condition involving $J_0(x)$, but a very good match is observed with respect to the condition involving $|J_1(x)|$. In addition, a proper tuning of the vertical post height helps to adjust the relative phase between the horizontal and vertical field components.

This exploitation of folded parasitics is quite different from the approach in [8], which follows the concept of polarizers [21, Sec. 23-5], i.e., long parallel rods (here dielectric rods with square cross section) placed at an angle so as to rotate the polarization of the incident field.

Finally, since the radiation at the low elevation angle is one of the main purposes of the proposed structure, it is interesting to note that the finite ground plane allows improving the AR at grazing incidence. In this respect, one should mention that an infinite ground plane necessarily leads to purely vertical polarization (infinite AR) at zero elevation ($\theta = 90^\circ$), while the example that is described in Section V has an AR between 1.8 and 4.0 dB at zero elevation.

B. Antenna Design

The main characteristic dimensions of the parasitic elements correspond to their distance from the monopole, the lengths of the two vertical parts, and the length of the horizontal parts. The cross section of the parasitic elements plays a secondary but nonnegligible role. This cross section is mainly governed by mechanical strength. The little horizontal bar at the foot of the parasitic element can marginally improve the antenna radiation performance. It also contributes to the strength of

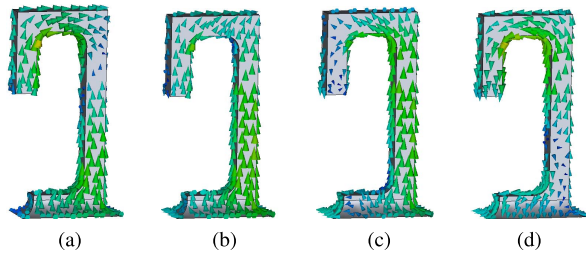


Fig. 4. Current distribution on the single element at (a) $t = 0$, (b) $t = T/8$, (c) $t = T/4$, and (d) $t = 3T/8$ (T is the time period at 8.428 GHz) as obtained with the CST Microwave Studio [22].

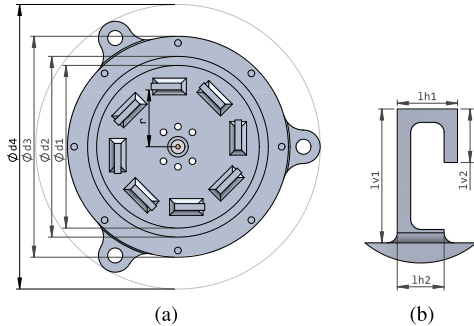


Fig. 5. Dimensions of the monopole parasitic antenna. (a) Top view. (b) Parasitic element.

the structure. Given the relatively simple shape of the parasitic elements, the whole conducting structure can be milled out of a single block of aluminum or can be produced through an additive manufacturing process.

The design used as a reference in this paper is intended for operation at the X-band (8.4–8.45 GHz) with a central frequency of 8.428 GHz. The design has the following gain requirements: at least 4 dB for $35^\circ \leq \theta \leq 60^\circ$ and 3 dB for $60^\circ \leq \theta \leq 70^\circ$. The AR should be at most 3 dB for $35^\circ \leq \theta \leq 70^\circ$.

Fig. 5 shows the dimensions of the monopole parasitic antenna along with those of a single parasitic element. Here, r denotes the separation between the parasitic elements and the monopole feed, and $(d2 - d1)/2$ indicates the gap in the choke ring. The three feet at the base of the antenna make it easy to mount the antenna atop a platform with nuts and bolts. To ease the fabrication with precision machining and to make the structure robust, the antenna has fillets around the base and the inner corners of the parasitic elements. All the fillets in the parasitic element (Fig. 5) have a radius of 1.5 mm. Fig. 6 shows the detailed view of the vertical section of the choke ring (left) and that of the monopole (right). The choke ring parameters, dt and dc , are measured from the base of the parasitic elements. The monopole height is given by lm , and the sleeve length, computed from the base of the parasitic elements, is given by ls . The thickness of the base plate, on which the parasitic elements rest and the monopole feed can be screwed, is given by tg . A dielectric tube acts as a spacer to hold the monopole in place. In practice, an SMA connector with extended central contact can replace the monopole and dielectric tube, and the dielectric portion of the connector can be cut to the height of the base plate, tg . The diameter of

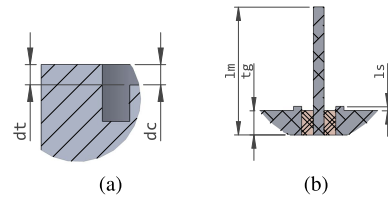


Fig. 6. Dimensions of (a) choke ring and (b) monopole feed.

TABLE I
DESIGN PARAMETERS OF THE ANTENNA

Parameter	Value (mm)	Parameter	Value (mm)
r	17	$lh1$	9
$d1$	48.6	$lh2$	7
$d2$	56	$lv1$	20
$d3$	66	$lv2$	8
$d4$	85	lm	15.9
dc	3.64	ls	0.5
dt	2	tg	3

the central connector is 1.3 mm, and the thickness of each of the parasitic elements is 2 mm. Table I summarizes the values used in the antenna design.

III. PARAMETRIC STUDY

Several parameters of the antenna play important roles in generating CP conical-beam. Understanding these different parameters is important to help design the antenna to meet any stringent specifications of CP conical beam patterns at any desired frequency.

The parameters under study are: separation between the monopole and the parasitic element, effect of the larger ground plane, and the different dimensions of the parasitic element. The length of the monopole is fixed at 15.9 mm, which is the length of a standard SMA connector with extended central contact. The length protruding out of the base plate is $lm - tg = 12.9$ mm. Without the parasitic elements, the antenna would resonate at 5.8 GHz instead of 8.4 GHz. For the parametric study, the mounting feet have been removed, and in some cases, also the fillets around the monopole elements. The mounting feet introduce some small ripple in the azimuthal gain, whereas the fillets have a negligible impact on antenna electromagnetic performance.

A. Monopole Height

A standard SMA connector can be directly screwed to feed the antenna, which makes the feed system extremely simple. However, it is possible to tune the antenna or improve its bandwidth with different monopole heights (lm). The -10 dB impedance bandwidth is, on average, around 7.6%.

B. Monopole to Parasitic Element Separation

The monopole to parasitic element separation (r) is another important parameter for tuning the antenna frequency (Fig. 7). However, the antenna patterns need to be reoptimized at

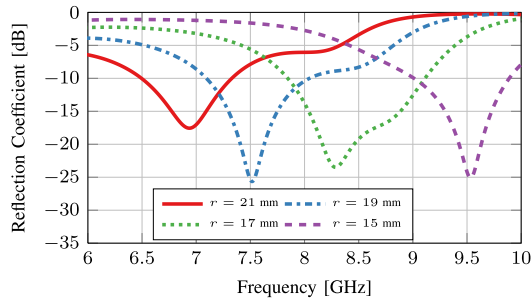


Fig. 7. Reflection coefficient for a different separation between the monopole and the parasitic elements.

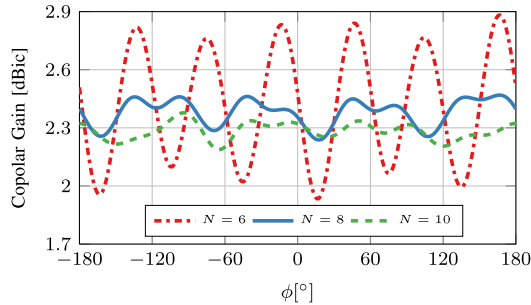


Fig. 8. Azimuthal gain variations at $\theta = 70^\circ$ for different numbers of parasitic elements.

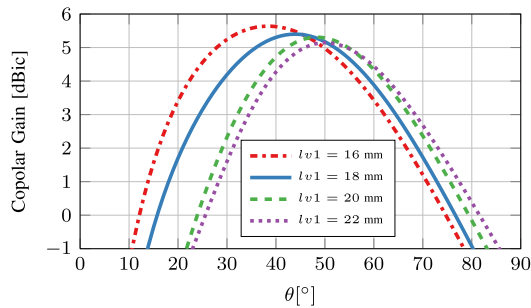


Fig. 9. Copolar gain at $\phi = 0^\circ$ for different heights ($lv1$) of parasitic elements.

the shifted frequency by modifying all the parameters of the parasitic elements. In terms of impedance matching, roughly speaking, the frequency is inversely proportional to r .

C. Parasitic Element Parameters

The number of parasitic elements mainly affects the azimuthal gain symmetry (Fig. 8). With a large number of elements, the gain variation over the azimuth decreases. This does not have a significant impact on the reflection coefficient nor on the AR.

Even though the vertical length, $lv1$, does not affect the reflection coefficient very much, it plays a role in improving gain at different elevation angles (Fig. 10). A higher element favors increased gain at lower elevation angles. The other vertical length, $lv2$, however, affects the reflection coefficient (Fig. 9) but does not affect the overall gain at any elevation angle. This length is crucial to create a balance in the vertical polarization and, thus, impacts more on the AR.

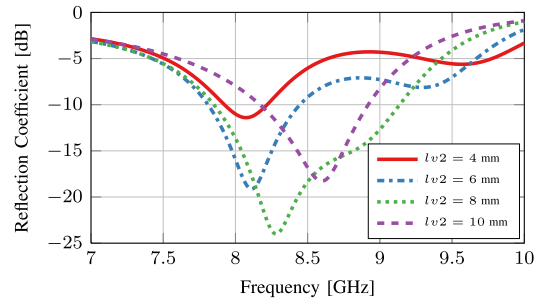


Fig. 10. Reflection coefficient for different heights ($lv2$) of parasitic elements.

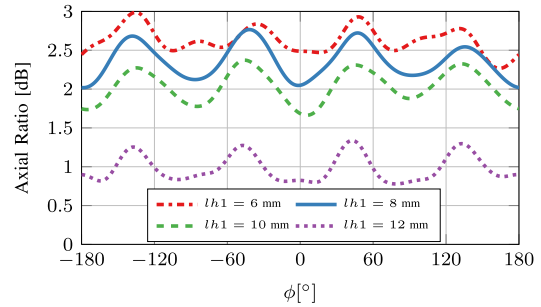


Fig. 11. AR at $\theta = 70^\circ$ for different horizontal lengths ($lh1$) of parasitic elements.

The horizontal length, $lh1$, contributes again in balancing the horizontal and vertical polarizations (reducing the AR, see Fig. 11) and also affects the reflection coefficient.

IV. GAIN OPTIMIZATION AND COMPARISON

The proposed design has the flexibility to change the angle of maximum gain. Depending on the applications, the antenna can be optimized to perform well with patterns pointed at a range of elevation angles, θ_{max} , from 35° to 70° .

Table II summarizes the most important performance metrics at the intermediate angles between 35° and 70° at 8.428 GHz, and compares these metrics to those obtained in the literature. Note that the values given in [4] are peak directivity values. As such, they do not consider the dielectric and feed network losses. Some modes proposed in [4] require excitation pins that are unevenly distributed along the patch azimuth. This may lead to large azimuthal variations in the radiation pattern and difficulties to balance and match the feeding network [25]. In this respect, we have to consider the peak directivity provided in [4] for the TM_{41} mode (4 dB, see the bottom-right value in Table II) as quite theoretical [26].

In terms of gain performance, the proposed design remains competitive with what is found in the literature regarding low-elevation conical patterns with circular polarization, as summarized in Table II. In [10], a maximum gain of 7.2 dBic is attained only for a ground plane size of 10λ while for 2λ , the achieved gain is 7 dBic for $\theta_{max} = 35^\circ$. Our design attains a 7 dBic gain at $\theta_{max} = 35^\circ$ for a ground plane of 3λ . While the beam-pointing angle in [15] can vary from 0° to 90° , the gain value is given only for 45° . In [23], a crossed drooping dipole antenna with four arms is used to attain a maximum gain of 4.8 dBic, but it has azimuthal gain variations

TABLE II
ANTENNA GAIN OPTIMIZATION AND COMPARISON WITH PUBLISHED DESIGNS

Prototype					References				
θ_{max}	Gain (dBic) [min, max]	AR BW* (%)	S11 BW* (%)	3-dB Beamwidth	θ_{max}	Gain (dBic)	AR BW* (%)	S11 BW* (%)	[Reference] Antenna Type
35°	[7.02, 7.21]	21.85	10.52	36°	35°	7.2	24.8	19.9	[10] Elliptical slot
50°	[6.47, 6.70]	14.06	13.95	30°	33°	5.5	28.2	28.3	[2] Multilayer patch
60°	[5.13, 5.35]	5.15	5.22	39°	46°	6.5	-	2.66	[24] Multilayer patch
70°	[4.06, 4.30]	7.27	5.42	25°	45°	5.8	11.25	8.7	[15] Conical slot array
					60°	4.8	-	-	[23] Drooping dipole
					70°	4.0 [‡]	-	-	[4] Circular patch

*Bandwidth, [‡]Directivity

TABLE III
PARAMETER VALUES USED IN GAIN OPTIMIZATION

Parameters (mm)	Angle of Maximum Gain (θ_{max})			
	35°	50°	60°	70°
r	18.42	17.02	33.31	33.39
$d1$	70.84	70.84	104.62	110.77
$d2$	92.54	97.0	125.37	120.77
$d3$	106.0	120.0	137.0	144.0
dc	12.0	12.82	6.0	6.0
dt	0.0	-0.94	3.0	-3.0
$lh1$	8.55	7.37	11.5	12.0
$lh2$	11.0	4.1	12.0	8.0
$lv1$	12.55	20.5	23.0	24.0
$lv2$	5.78	7.0	2.0	2.0
N^*	10	10	13	14

*Dimensionless

larger than 2 dB, while our design has gain ripple smaller than 0.22 dB.

Table III gives the parameter values used to obtain the performance metrics of Table II. Some parameters, such as lm , ls , and tg , have the same values as in Table I. The simulated results for the antennas optimized for a given θ_{max} angle are shown in Figs. 12–14. While the gain optimization at a higher elevation is easier, the gain at lower elevation suffers from having additional energy spilled over due to sidelobes at higher elevations (Fig. 12). The antenna diameter is relatively large (almost 4λ) for the design optimized for low elevation angles. This probably explains the smaller bandwidth for grazing angles, given the larger phase roll with a frequency between the feeding pin and the parasitic element, which is located further away. In Fig. 3, the vertical lines show how the different designs displayed in columns of Table III comply with the rules established using (2) and (5), which limit the impact of the vertical parts of the parasitics on the antenna polarization. We can see that in each design, the corresponding value of $x = ka \sin \theta$ is close to zero of $J_0(x)$ and close to a maximum of $|J_1(x)|$. As explained in Section II-A, those two mathematical conditions allow a good polarization balance. We observe the existence of two modes, with values of parameter x clustered in two domains. Finally, the vertical line labeled with $\theta = 23^\circ$ in Fig. 3 corresponds to a secondary peak appearing in the radiation pattern of the antenna optimized for radiation toward $\theta = 70^\circ$ (see Fig. 12).

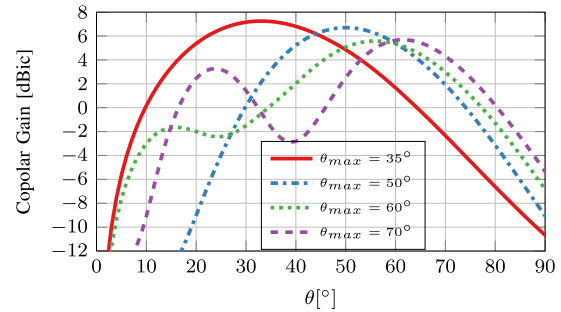


Fig. 12. Best case copolar gains of the gain-optimized antennas at 8.428 GHz.

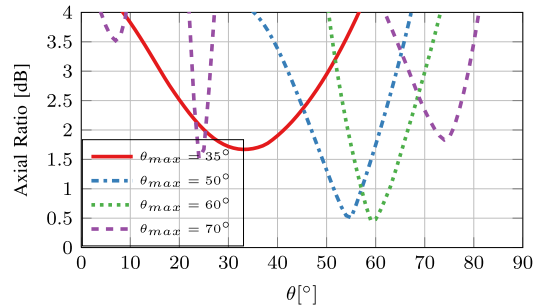


Fig. 13. Worst case AR of the gain-optimized antennas at 8.428 GHz.

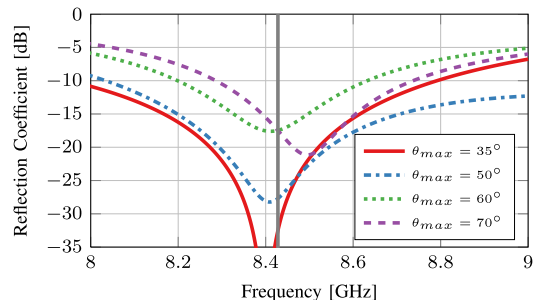


Fig. 14. Reflection coefficients of the gain-optimized antennas at 8.428 GHz.

V. EXPERIMENTAL VALIDATION

For rapid prototyping, the antenna was fabricated using metal additive manufacturing (Fig. 15). While a complex feed structure is not necessary for this type of antenna, a semirigid cable assembly was built [Fig. 15(b)] to make it possible to

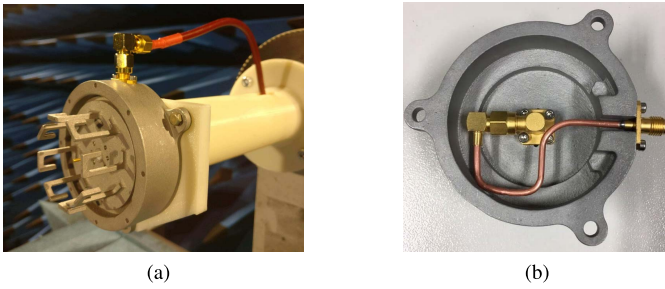


Fig. 15. 3-D printed prototype antenna (a) mounted in the anechoic chamber and (b) with the semirigid cable feed assembly.

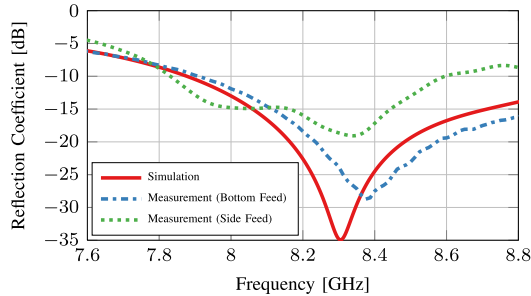


Fig. 16. Reflection coefficient of the measured prototype.

feed the antenna from a lateral connector and to make calibration easier during the measurement activity. For the measurement of the reflection coefficient (Fig. 16), two feed setups are considered: a direct bottom feed using a straight SMA connector with extended central contact and a side feed using a semirigid cable assembly. The latter consists of a right-angle plug, a 0.085" RG405 semirigid cable, and a two-hole flange jack connected to a right-angle SMA connector with extended central contact/conductor acting as the monopole. The curved semirigid cable was required to accommodate the assembly and also to meet the extra cable length requirements for space applications. This solution was, however, deemed too lossy and prone to suboptimal performance in case of large temperature fluctuations. Thus, it was replaced with a square coaxial line, as described in Section VI. The measurement result with the bottom feed shows close correspondence with the simulated result (Fig. 16). The difference is probably due to the manufacturing imperfections. The measurement result with the semirigid cable assembly is quite different from the simulated result because of the change in the cable properties resulting from the sharp bends, as could be verified through the S-parameter measurement of the semirigid cable taken in isolation. In this case, the effect of the cable assembly is not considered in the simulation. The imperfections of that cable are not expected to impact the measured directivity. Fig. 17 shows the simulated radiation patterns of the 3-D printed antenna over different azimuthal angles.

Fig. 18 shows the best and worst case copolar [right-hand circular polarization, (RHCP)] gains at each elevation angle (where the gain is positive in decibels) over the whole azimuthal plane. The best case gain means the largest value over all azimuth angles, for each angle θ of interest. Similarly,

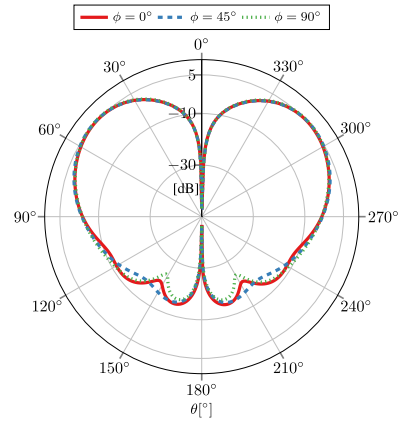


Fig. 17. Simulated copolar gain patterns of the 3-D printed prototype at 8.428 GHz over different azimuth angles.

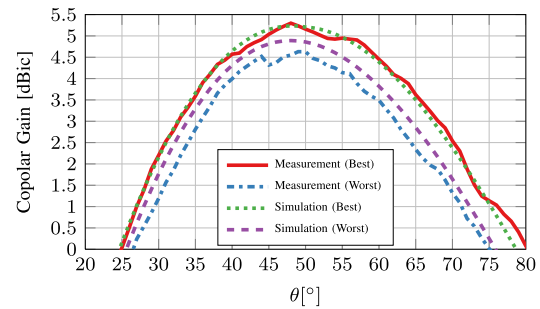


Fig. 18. Best and worst case copolar gains of the prototype at 8.428 GHz.

the worst case gain refers to the lowest gain over azimuth. This plot gives the best and worst values of copolar gain (RHCP) for the elevation angles in the upper hemisphere [0° – 90°] at 8.428 GHz. The measurement results show a good correspondence with the simulation results (see Fig. 18). The azimuthal gain variations in the measurement are poorer compared to the simulated ones but are still smaller than 1 dB from $\theta = 30^\circ$ to $\theta = 70^\circ$.

Fig. 19 shows the worst case AR of the simulated and 3-D printed prototype. The worst case AR means the largest value over all azimuthal angles for the angle θ of interest. AR is lower than 3 dB from $\theta = 39^\circ$ to $\theta = 68^\circ$. This difference could be due to the scattering by the antenna holder designed for the measurement purpose.

VI. APPLICATION TO A MARTIAN TRANSPONDER

The all-metal parasitic radiator is attractive for space applications, given its good mechanical strength and optimal antenna gain performance even at extreme temperatures. Indeed, the thermoelastic changes in the dielectric substrate can have a drastic effect on antenna performance because of the thermal expansion mismatch between different materials; this worsens if numerous vias are needed in a multilayered stackup.

The proposed antenna is considered for use in the Lander Radioscience (LaRa) instrument aboard a Russian surface

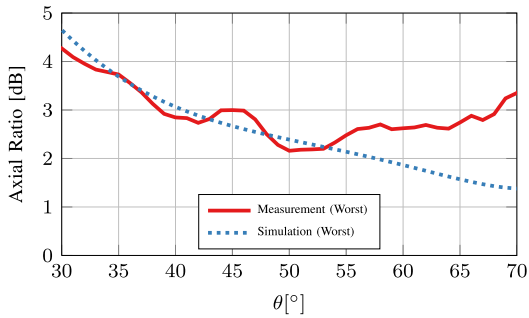


Fig. 19. Worst case AR of the prototype at 8.428 GHz.

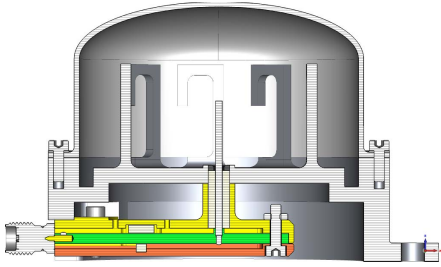


Fig. 20. Section view of the LaRa antenna with the radome and square coaxial feeding line.

platform of the ExoMars 2020 mission to Mars. The mission will also deliver a European rover to the surface for studying the possibilities of life on the red planet. LaRa aims to understand the deep inner structure of the planet to reveal its origin and evolution, through precise measurements of the planet's rotation and orientation by monitoring the two-way Doppler shifts in frequency [27]. An X-band signal from the Earth ground stations will be received by the LaRa receive antennas, going through a LaRa transponder electronics box, up-converting the carrier frequency with phase coherence and transmitting it directly back to Earth with one of the other LaRa transmit antennas. The phased-array design [28] has been ruled out because of the robustness requirement of the antenna. According to the observation requirements, the antennas should have an optimal gain between 35° and 45° from the surface of the platform, i.e., elevation (or $\theta = 45^\circ$ to 55°), low-azimuthal gain variations, and low AR. The envelope requirement puts the maximum antenna size at 85 mm (Table I), which imposes additional constraints on pattern optimization.

Apart from the core aluminum housing of the antenna described in Section II, the LaRa antennas (Fig. 20) have additional components for protection from the Martian environment, and improved manufacturing processes to adhere to the space standards. Among the most significant is a radome atop the housing, which affects the circular polarization purity but, on the other hand, reduces azimuthal gain variations. The outer wall of the choke ring is made relatively thick so as to support a radome. The antenna performance has been optimized in the presence of the radome. The semirigid cable assembly used to feed the structure, as described in Section V, is replaced by a square coaxial transmission line [29], which is mostly filled with air and two supporting dielectric

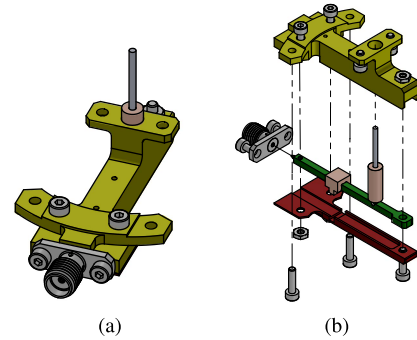


Fig. 21. LaRa antenna square coaxial feeding line showing (a) assembled view and (b) exploded view.

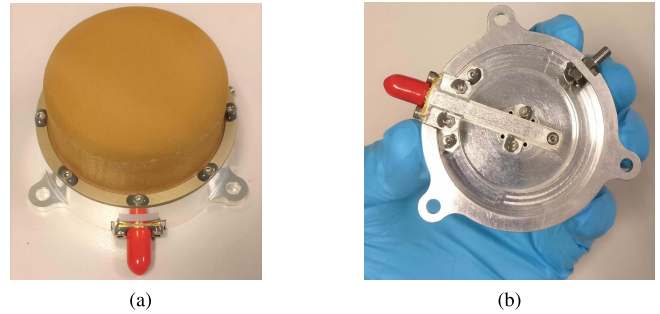


Fig. 22. Manufactured LaRa antenna. (a) Top view with the radome. (b) Bottom view with the square coaxial feeding line.

cylinders (see Fig. 21). The benefit of using the square coaxial transmission line is its robustness to temperature variations and extremely low RF loss in the feed assembly. The square coaxial feeding line [Fig. 22(b)] is made out of aluminum, assembled, and screwed according to Fig. 21(b). The long horizontal central contact is soldered to the vertical monopole. From the soldering point, a quarter-wavelength horizontal extension continues [Fig. 21(b)] and is electrically connected to the housing. This extension ensures a good mechanical strength without a significant effect at the X-band (virtual open circuit in parallel). This extension also serves as a grounding to avoid electrostatic charging of the center conductor.

A. Measurement Results

The LaRa antenna housing was manufactured out of a single block of aluminum using precision machining. The radome was made of a fiberglass composite material (Hex-Ply 8552 resin system with woven glass fiber) having a thickness of 1 mm [Fig. 22(a)]. The screws are all staked with a Scotch-Weld epoxy adhesive. The pattern measurement was carried out in an anechoic chamber using a SATIMO quad-ridge reference horn QH800 at a distance of 3.94 m from the test antenna. The test antenna was rotated with a turntable, while the reference horn was fixed.

The measured reflection coefficient seems to vary compared to the simulated one (see Fig. 23). The measured impedance bandwidth for $|S_{11}| < -10$ dB is 14.9%, whereas the simulated impedance bandwidth is 10.7%. This can be explained

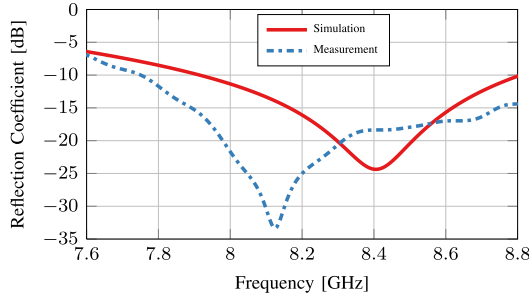


Fig. 23. Reflection coefficient of the measured LaRa antenna.

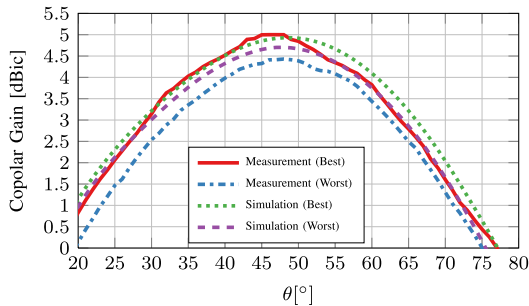


Fig. 24. Best and worst case copolar gains of the LaRa antenna at 8.428 GHz.

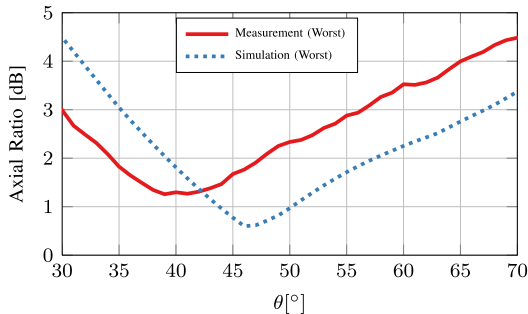


Fig. 25. Worst case AR of the LaRa antenna at 8.428 GHz.

by the tight manufacturing tolerance on the square coaxial feeding line (order of $30 \mu\text{m}$, difficult to attain in practice). Moreover, the radome has a rough surface, which could play a minor role in the change in performance. The RHCP copolar gain is shown in Fig. 24. The measured gain shows a good correspondence with the simulated result, although the worst case gain is slightly deteriorated. This could be because of using an inaccurate model in the simulation for the radome composite material, whose dielectric properties were not accurately known beforehand. A similar trend is noted in the worst case AR plot of Fig. 25, where the antenna performs better in higher elevation (or lower θ). The simulated AR bandwidth for $\text{AR} < 3 \text{ dB}$ at the angle of maximum gain, $\theta = 50^\circ$, is found to be 20.4%.

VII. CONCLUSION

This paper presents a novel metallic antenna based on a monopole feed surrounded by several gamma-shaped metallic

parasitic elements, which produces a circularly polarized conical beam. The distinct shape of the parasitic element with its horizontal and vertical arms helps create a balance in the horizontal and vertical currents responsible for generating circular polarization. We explained how an appropriate choice of the antenna radius enables limiting the fields radiated by the vertical parts of parasitics while they can conduct current from the ground plane to the horizontal arms. The antenna is suitable for use under harsh environmental conditions, and is easily optimized for high performance at different elevation angles. Given its 3-D structure, the antenna can offer high gain at low elevation. Simulation results show that the gain above 4 dB at $\theta = 70^\circ$ is possible. Both the additive manufacturing prototype and the precision machining model show positive experimental results.

ACKNOWLEDGMENT

The authors would like to thank the LaRa Team at Antwerp Space for their support, M. Van Gijssels for his mechanical design support, J.-F. Boone for project management, and B. Desoete for material selection and fabrication via Maex. They would also like to thank J. I. Echeveste for preliminary design support.

REFERENCES

- [1] T. Manabe *et al.*, "Polarization dependence of multipath propagation and high-speed transmission characteristics of indoor millimeter-wave channel at 60 GHz," *IEEE Trans. Veh. Technol.*, vol. 44, no. 2, pp. 268–274, May 1995.
- [2] K. L. Lau and K. M. Luk, "A wideband circularly polarized conical-beam patch antenna," *IEEE Trans. Antennas Propag.*, vol. 54, no. 5, pp. 1591–1594, May 2006.
- [3] J. Wick, "Sense reversal of circularly polarized waves on earth-space links," *IEEE Trans. Antennas Propag.*, vol. AP-15, no. 6, pp. 828–829, Nov. 1967.
- [4] J. Huang, "Circularly polarized conical patterns from circular microstrip antennas," *IEEE Trans. Antennas Propag.*, vol. AP-32, no. 9, pp. 991–994, Sep. 1984.
- [5] H. Kawakami, G. Sato, and R. Wakabayashi, "Research on circularly polarized conical-beam antennas," *IEEE Antennas Propag. Mag.*, vol. 39, no. 3, pp. 27–39, Jun. 1997.
- [6] S.-S. Qi, W. Wu, and D.-G. Fang, "Singly-fed circularly polarized circular aperture antenna with conical beam," *IEEE Trans. Antennas Propag.*, vol. 61, no. 6, pp. 3345–3349, Jun. 2013.
- [7] H. Nakano, H. Oyanagi, and J. Yamauchi, "A wideband circularly polarized conical beam from a two-arm spiral antenna excited in phase," *IEEE Trans. Antennas Propag.*, vol. 59, no. 10, pp. 3518–3525, Oct. 2011.
- [8] Y. M. Pan and K. W. Leung, "Wideband circularly polarized dielectric bird-nest antenna with conical radiation pattern," *IEEE Trans. Antennas Propag.*, vol. 61, no. 2, pp. 563–570, Feb. 2013.
- [9] W. Lin and H. Wong, "Circularly polarized conical-beam antenna with wide bandwidth and low profile," *IEEE Trans. Antennas Propag.*, vol. 62, no. 12, pp. 5974–5982, Dec. 2014.
- [10] D. Yu, S.-X. Gong, Y.-T. Wan, and W. Jiang, "Wideband conical-beam circularly polarized microstrip antenna for large ground plane," *IEEE Trans. Antennas Propag.*, vol. 63, no. 10, pp. 4614–4619, Oct. 2015.
- [11] H. Xu, J. Zhou, Q. Wu, Z. Yu, and W. Hong, "Wideband low-profile SIW cavity-backed circularly polarized antenna with high-gain and conical-beam radiation," *IEEE Trans. Antennas Propag.*, vol. 66, no. 3, pp. 1179–1188, Mar. 2018.
- [12] S. V. Kumar and A. R. Harish, "Generation of circularly polarized conical beam pattern using torus knot antenna," *IEEE Trans. Antennas Propag.*, vol. 65, no. 11, pp. 5740–5746, Nov. 2017.
- [13] H. Ohmine, Y. Sunahara, M. Matsunaga, and S. Mano, "Car-top annular-ring microstrip antenna," in *Proc. Int. Symp. Antennas Propag. Soc.*, Dallas, TX, USA, vol. 3, May 1990, pp. 1136–1139.
- [14] H. Ohmine, Y. Sunahara, and M. Matsunaga, "An annular-ring microstrip antenna fed by a co-planar feed circuit for mobile satellite communication use," *IEEE Trans. Antennas Propag.*, vol. 45, no. 6, pp. 1001–1008, Jun. 1997.

- [15] G. Chenhu *et al.*, "Truncated circular cone slot antenna array that radiates a circularly polarized conical beam," *IEEE Antennas Wireless Propag. Lett.*, vol. 16, pp. 2574–2577, 2017.
- [16] R. Schlub, J. Lu, and T. Ohira, "Seven-element ground skirt monopole ESPAR antenna design from a genetic algorithm and the finite element method," *IEEE Trans. Antennas Propag.*, vol. 51, no. 11, pp. 3033–3039, Nov. 2003.
- [17] H.-T. Liu, S. Gao, and T.-H. Loh, "Electrically small and low cost smart antenna for wireless communication," *IEEE Trans. Antennas Propag.*, vol. 60, no. 3, pp. 1540–1549, Mar. 2012.
- [18] J. Tranquilla, J. P. Carr, and H. M. Al-Rizzo, "Analysis of a choke ring groundplane for multipath control in Global Positioning System (GPS) applications," *IEEE Trans. Antennas Propag.*, vol. 42, no. 7, pp. 905–911, Jul. 1994.
- [19] F. Scire-Scappuzzo and S. N. Makarov, "A low-multipath wide-band GPS antenna with cutoff or non-cutoff corrugated ground plane," *IEEE Trans. Antennas Propag.*, vol. 57, no. 1, pp. 33–46, Jan. 2009.
- [20] Z. Shen and R. H. MacPhie, "Theoretical modeling of multi-sleeve monopole antennas," *Prog. Electromagn. Res.*, vol. 31, pp. 31–54, Jan. 2001.
- [21] R. C. Johnson and H. Jasik, *Antenna Engineering Handbook*. New York, NY, USA: McGraw-Hill, 1993.
- [22] *CST Studio Suite Electromagnetic and Multiphysics Software*, Dassault Systèmes, Vélizy-Villacoublay, France, 2017.
- [23] T. K. Wu and J. Huang, "Low-cost antennas for direct broadcast satellite radio," *Microw. Opt. Technol. Lett.*, vol. 7, no. 10, pp. 440–444, Jul. 1994.
- [24] X. Bai, X. Liang, M. Li, B. Zhou, J. Geng, and R. Jin, "Dual-circularly polarized conical-beam microstrip antenna," *IEEE Antennas Wireless Propag. Lett.*, vol. 14, pp. 482–485, 2015.
- [25] J. C. Batchelor and R. J. Langley, "Microstrip ring antennas operating at higher order modes for mobile communications," *IEE Proc. Microw., Antennas Propag.*, vol. 142, no. 2, pp. 151–155, Apr. 1995.
- [26] F. Tiezzi and S. Vaccaro, "Gain considerations of circular and annular printed antennas operating at higher order resonant modes," in *Proc. Int. ITG-Conf. Antennas INICA*, Berlin, Germany, 2003, pp. 205–208.
- [27] V. Dehant *et al.*, "Lander radioscience for obtaining the rotation and orientation of Mars," *Planetary Space Sci.*, vol. 57, nos. 8–9, pp. 1050–1067, Jul. 2009.
- [28] S. Karki, C. Craeye, M. Mitrovic, and V. Dehant, "A conical frustum-type array devoted to a Mars-based transponder," in *Proc. 10th Eur. Conf. Antennas Propag. (EuCAP)*, Davos, Switzerland, Apr. 2016, pp. 1–4.
- [29] M. Lukic, S. Rondineau, Z. Popovic, and S. Filipovic, "Modeling of realistic rectangular μ -coaxial lines," *IEEE Trans. Microw. Theory Techn.*, vol. 54, no. 5, pp. 2068–2076, May 2006.



Sumit Karki received the bachelor's degree in electrical and electronic engineering from Kathmandu University, Dhulikhel, Nepal, in 2010, and the master's degree in research on information and communication technologies from the Université catholique de Louvain, Louvain-la-Neuve, Belgium, and the Universitat Politècnica de Catalunya, Barcelona, Spain, on an Erasmus Mundus grant to pursue the double degree, in 2013, and the Ph.D. degree from the Université catholique de Louvain FRIA grant in 2018.

Since 2019, he has been an RF Engineer with Aerospacelab, Belgium. His current interests include space antenna design, RF front-end design, and fast numerical techniques for antenna analysis.



Marco Sabbadini received the M.Sc. degree from Università di Roma Sapienza, Roma, Italy, in 1983.

From 1983 to 1988, he was with the Antenna Group, Thales Alenia Space Italy, Rome, Italy. From 1988 to 2018, he was with European Space Agency, ESTEC, Noordwijk, The Netherlands. He currently collaborates with Università di Siena, Italy. His current research interests include computational electromagnetics and computer-aided antenna engineering tools, and the development of creative solutions in space antenna technology, most notably, the recent development of modulated metasurface antennas. Finally, he is involved in the assessment of the impact of the plasma generated by shock waves during hypersonic atmospheric reentry on antenna radiation patterns.



Khaldoun Alkhalifeh (M'16) was born in Aleppo, Syria, in 1981. He received the Diploma degree in electrical and electronic engineering from the Faculty of Electrical and Electronic Engineering, Aleppo University, Aleppo, in 2006, and the master's degree in microwave and telecommunications and the Ph.D. degree in antenna engineering from the Université catholique de Louvain (UCL), Louvain-la-Neuve, Belgium, in 2010 and 2017, respectively.

Since 2017, he has been a Research Associate with the Antenna Research Group, Institute of Information and Communication Technologies, Electronics and Applied Mathematics, UCL. His current research interests include multiband antenna array design and analysis, ground penetrating radar applications, fast numerical methods for electromagnetic fields in finite periodic structures, and near-field imaging.



Christophe Craeye (M'98–SM'11) was born in Belgium, in 1971. He received the master's degree in electrical engineering, the B.Phil. degree, and the Ph.D. degree in applied sciences from the Université catholique de Louvain (UCL), Louvain-la-Neuve, Belgium, in 1994, 1994, and 1998, respectively.

From 1994 to 1999, he was a Teaching Assistant with UCL, where he carried out research on the radar signature of the sea surface perturbed by rain, in collaboration with NASA and ESA. From 1999 to 2001, he was a Post-Doctoral Researcher with the Eindhoven University of Technology, Eindhoven, The Netherlands. He was with the University of Massachusetts at Amherst, Amherst, MA, USA, in 1999. He was with the Netherlands Institute for Research in Astronomy, Dwingeloo, The Netherlands, in 2001. In 2002, he started an antenna research activity with UCL, where he is currently a Professor. He was with the Astrophysics and Detectors Group, University of Cambridge, Cambridge, U.K., in 2011. His research was funded by the Region Wallonne, European Commission, ESA, Fonds de la Recherche Scientifique, Bruxelles, Belgium, and UCL. His current research interests include mutual coupling, finite antenna arrays, wideband antennas, small antennas, metamaterials, fast physical optics and numerical methods for fields in periodic media, and with applications to communication and sensing systems.

Dr. Craeye received the 2005–2008 Georges Vanderlinden Prize from the Belgian Royal Academy of Sciences in 2009. He was an Associate Editor of the IEEE TRANSACTIONS ON ANTENNAS AND PROPAGATION from 2004 to 2010 and for the IEEE ANTENNAS AND WIRELESS PROPAGATION LETTERS from 2011 to 2017.